Cancer Research

Nedd4-Binding Protein 1 and TNFAIP3-Interacting Protein 1 Control MHC-1 Display in Neuroblastoma

Lotte Spel[1], Joppe Nieuwenhuis[2,3], Rianne Haarsma[1], Elmer Stickel[2], Onno B. Bleijerveld[4], Maarten Altelaar[4,5], Jaap Jan Boelens[1], Thijn R. Brummelkamp[2,3,6,7], Stefan Nierkens[1], and Marianne Boes[1]

Abstract

Neuroblastoma is the second most common tumor in children. The cause of neuroblastoma is thought to lie in aberrant development of embryonic neural crest cells and is accompanied by low MHC-1 expression and suppression of the NF-κB transcription factor, thereby gearing cells toward escape from immunosurveillance. Here, we assess regulation of the MHC-1 gene in neuroblastoma to enhance its immunogenic potential for therapeutic T-cell targeting. A genome-wide CRISPR screen identified N4BP1 and TNIP1 as inhibitory factors of NF-κB-mediated MHC-1 expression in neuroblastoma. Patients with advanced stage neuroblastoma who expressed high levels of TNIP1 and N4BP1 exhibited worse overall survival. Depletion of N4BP1 or TNIP1 increased NF-κB and MHC-1 expression and stimulated recognition by antigen-specific $CD8^+$ T cells. We confirmed that TNIP1 inhibited canonical NF-κB member RelA by preventing activation of the RelA/p50 NF-κB dimer. Furthermore, N4BP1 inhibited both canonical and noncanonical NF-κB through binding of deubiquitinating enzyme CEZANNE, resulting in stabilization of TRAF3 and degradation of NF-κB-inducing kinase NIK. These data suggest that N4BP1/CEZANNE or TNIP1 may be candidate targets for immunotherapy in neuroblastoma tumors and should lift NF-κB suppression, thereby triggering increased peptide/MHC1-mediated tumor reactivity to enhance therapeutic T-cell targeting.

Significance: Aberrant regulation of NF-κB and MHC-1 in neuroblastoma tumors provides new targets for immunotherapeutic approaches against neuroblastoma. *Cancer Res; 78(23); 6621–31. ©2018 AACR.*

Introduction

Neuroblastoma accounts for 15% of pediatric cancer mortality (1–3). It is the most common solid tumor in children with survival rates of merely 40% in advanced stage (stage 4) disease (1). Neuroblastoma is an embryonic cancer that originates from neural crest cells. The mutational burden of neuroblastoma tumors is low (4, 5), hence so far, no neo-antigens have been reported for neuroblastoma. Instead, expression of cancer/testis antigens have been described in neuroblastoma (6–8) reflecting the embryonically undifferentiated status of this type of tumor.

Immunotherapy for stage 4 neuroblastoma gains traction. Currently, antibody therapy targeting the neuroblastoma-specific surface disialoganglioside GD2 is standard protocol succeeding radiotherapy, chemotherapy, surgery, and autologous stem cell transplantation. In addition, various immunotherapies are in trial stages (9, 10). However, due to its low immunogenicity (11, 12), neuroblastoma tumors continue to pose a challenge for immunotherapeutic approaches. Neuroblastoma typically presents with extremely low levels of MHC class 1 (MHC-1), especially in stage 4 patients (7), preventing recognition and lysis of neuroblastoma cells by cytotoxic T lymphocytes (CTL).

Unique for neuroblastoma is the abnormally low levels of NF-κB protein that have been reported (13, 14), which sets neuroblastoma aside from all other solid tumors in which NF-κB is usually constitutively active (15). MHC-1 levels in neuroblastoma are, however, controlled by NF-κB (16). Activation of NF-κB induces transient MHC-1 membrane expression (13, 14, 17) that facilitates recognition by CTLs *in vitro* (13, 18–20), underscoring that reconstitution of MHC-1 by activation of the NF-κB pathway in these tumors might increase their immunogenicity.

In this study, we aimed to identify target proteins that control peptide/MHC-1 display in neuroblastoma by performing a genome-wide CRISPR knockout screen combining NF-κB activity and cell-surface MHC-1 membrane expression. We show that both canonical and noncanonical NF-κB may contribute to

[1]Laboratory of Translational Immunology, University Medical Center Utrecht, Utrecht, the Netherlands. [2]Department of Biochemistry, Netherlands Cancer Institute, Amsterdam, the Netherlands. [3]Oncode Institute, Netherlands Cancer Institute, Amsterdam, the Netherlands. [4]Proteomics facility, Netherlands Cancer Institute, Amsterdam, the Netherlands. [5]Biomolecular Mass Spectrometry and Proteomics, Utrecht Institute for Pharmaceutical Sciences, Utrecht, the Netherlands. [6]CeMM Research Center for Molecular Medicine of the Austrian Academy of Sciences, Vienna, Austria. [7]Cancergenomics.nl, Amsterdam, the Netherlands.

Note: Supplementary data for this article are available at Cancer Research Online (http://cancerres.aacrjournals.org/).

L. Spel, J. Nieuwenhuis, S. Nierkens, and M. Boes contributed equally to the article.

Corresponding Author: Marianne Boes, University Medical Center Utrecht, Heidelberglaan 100, 3584 EA Utrecht, the Netherlands. Phone: 31-88-755-4982; Fax: 31-88-755-5350; E-mail: M.L.Boes@umcutrecht.nl

doi: 10.1158/0008-5472.CAN-18-0545

©2018 American Association for Cancer Research.

Downloaded from http://aacrjournals.org/cancerres/article-pdf/78/23/6621/2601371/6621.pdf by guest on 12 October 2024

neuroblastoma immunogenic display and give mechanistic insight into the inhibitory mechanisms of these target proteins.

Materials and Methods

Cells and culture conditions

Neuroblastoma cell lines GIMEN, Sk-N-SH, SH-Sy5y Sk-N-BE and IMR32 were obtained via the Academic Medical Center of Amsterdam. Melanoma cell line BLM was obtained via the Radboud University Medical Center of Nijmegen. All cells were maintained in DMEM GlutaMAX supplemented with 10% FCS (Biowest), 50 U/mL penicillin (Life Technologies) and 50 μg/mL streptomycin (Life Technologies) and cultured at 37°C at 5% CO_2. Cell authentication was conducted through microarray analysis, performed at AMC (NCBI GEO Accession No. GSE 16476; http://www.ncbi.nlm.nih.gov/geo/) confirming neuroblastoma expression profiles, which were confirmed for selected neuroblastoma markers (*LIN28B*, *MYCN*, GD2, CD56, and CD81) by qPCR and/or FACS analysis when cells arrived at UMC Utrecht (2012). Cells were frozen in individual aliquots after less than 10 passages and tested regularly for *Mycoplasma* contamination.

Reagents and antibodies

Human recombinant TNF was purchased from Miltenyi. Decitabine, LPS and poly(I:C) were purchased from Sigma-Aldrich. Hoechst was purchased from Thermo Fisher Scientific. A list of all antibodies used can be found in the Supplementary Material.

Constructs and plasmids

For generating NF-κB reporter cells, a pTRH1 plasmid was used containing an NF-κB transcriptional response element (TRE) and a minimum CMV (mCMV) promoter followed by eGFP gene and upstream of the blasticidin S resistance gene (BSR) from *Bacillus cereus* (21). Clonal cell lines GIMEN ΔN4BP1 and ΔTNIP1, used in all follow-up experiments, were analyzed by TA-cloning (Strataclone PCR cloning kit, agilent #240205). At least 20 colonies were picked and subjected to sequencing to ensure no allele would be unannotated. For non-clonal cell lines, PCR product was subjected to sanger sequencing to obtain mutation profiles based on TIDE assay (22), using nested sanger sequencing primers Fw_N4BP1_seq: 5′-CTACAGCTCTCCAAGTGAAACATTTGAG-3′ and Fw_TNIP1_seq: 5′-CATTCTCCCACACTCGAGTGG- 3′. Information about gRNA sequences can be found in the Supplementary Material.

Flow cytometry

Cells were detached with trypsin (Life Technologies) and washed twice in PBS containing 2% FCS (Biowest) and 0.1% sodium azide (NaN3, Sigma-Aldrich). Next, antigen nonspecific binding was prevented by prior incubation of cells with 10% mouse serum (Fitzgerald). Cells were incubated with indicated anti-human antibodies for 30 minutes on ice and washed twice. In case of intracellular stainings, cells were fixed and permeabilized (Fix/Perm kit BD Biosciences) after surface staining and subsequently stained with indicated antibodies for 30 minutes on ice and washed twice. Cells were taken up in PBS (2% FCS/0,1% NaN3) to be used for measurement using either FACSCanto II or Fortessa with FACS Diva Version 6.13 (BD Biosciences). Analysis was done using FlowJo Version 10 software.

CRISPR screen analysis

An overview and detailed documentation of all commands and code used for the analysis can be found in the following Github repository: https://github.com/ElmerS/spel_et_al_2018. A summary of the procedure is written below. Sequence reads were uploaded to NIH Sequence Read Archive with access number: *SRP147989*.

Sequence read analysis

Raw sequence reads were extracted from the FASTQ files using AWK and subsequently, using regular expression in SED, sequences of 19-21b flanked by ACCG and GTT were distilled. Bowtie 1 (23) was used to align the reads to the lentivirus library in two consecutive rounds. In the first round, a single mismatch was allowed while demanding alignment to only a single guide. In the second round, the reads that aligned to multiple guides in the first round where re-aligned with a more stringent setting of zero mismatches to see if they could be aligned unambiguously.

Scoring sgRNA using differential expression analysis

Readcount files were generated from Bowtie output using a Bash script and differential expression analysis was carried out using the R package DESeq2 (24). The NF-$\kappa B^{low}MHC^{low}$ population from both screens were used as replicates for the low population and the NF-$\kappa B^{high}MHC^{high}$ populations as replicates for the high population. Differences in guide abundance between the low and high populations were tested using a Walt test with default size factor normalization of DESeq2. Shrinkage of Log2FoldChanges was applied. Guides with an FDR-corrected (Benjamini-Hochberg) *P* value that met the threshold of 0.05 were designated significant.

Candidate gene identification

Using a custom Python script, the number of guides per gene with a FDR corrected *P* value below or equal to the threshold was determined. Genes having at least three guides that met this threshold and which also showed identical directionality were selected as candidates. In total 9 genes fulfilled these criteria. To include the nontargeting control guides in this analysis, 167 hypothetical genes were randomly assigned 6 nontargeting control guides. For follow-up, those genes were selected that showed at least 2 significant gRNA hits above 500 reads.

Immunofluorescence microscopy

Cell were cultured in LabTek 8 well chambers in culture medium. Cells were subsequently washed and fixed for 10 minutes at RT using PBS supplemented with 4% formaldehyde. Cells were permeabilized and blocked for 60 minutes with PBS supplemented with 5% BSA and 0,3% Triton-X100. Next, slides were incubated with primary antibodies diluted in PBS supplemented with 1% BSA and 0.3% Triton-X100 for 16 hours. Cells were washed with PBS and incubated with secondary antibodies for 1 hour. After washing, slides mounted on a microscope slide using Mowiol 4-88 (Carl Roth, Germany). Samples were imaged using a Zeiss LSM710 confocal microscope equipped with a Plan-Apochromat 63 × 1.40 oil differential interference contrast M27 objective (Zeiss). Fluorescent signals were detected with PMTs set at the appropriate bandwidth using 633 nm helium neon laser for Alexa647. Images were processed using the Zeiss Enhanced Navigation (ZEN) 2009 software.

Downloaded from http://aacrjournals.org/cancerres/article-pdf/78/23/6621/2601371/6621.pdf by guest on 12 October 2024

Quantitative real-time PCR

Total RNA was isolated using RNA isolation columns (Qiagen) according to the manufacturer's instructions. cDNA was synthesized from 1 μg of total RNA using the iScript cDNA synthesis kit (Bio-Rad). Real-time PCR was performed using IQ SYBR Green PCR Supermix (Bio-Rad) and the CFX96 Touch Real-Time PCR Detection System (Bio-Rad), according to the manufacturer's instructions. PCR assays were done in triplicate. Data were calculated as values relative to GAPDH and further analyzed using GraphPad Prism 7.02.

T-cell activation assay

A HCMV pp65-specific $CD8^+$ T-cell clone was prepared previously. In brief, T cells from an HLA-A*0201+ donor were stained with HLA-A2/$pp65^{495\text{-}503}$ tetramers, and subsequently single-cell sorted in a 96-well plate (Thermo) containing irradiated B-LCL feeder cells (1×10^5 cells/mL, irradiated with 70 Gy) and PBMCs from 3 healthy donors (1×106 cells/mL, irradiated with 30 Gy). One μg/mL leucoagglutinin PHA-L (Sigma-Aldrich) and 120 U/mL of recombinant IL-2 (Immunotools) were added. T-cell clones specific to $pp65^{495\text{-}503}$ were selected using tetramer staining. Positive clones were restimulated and expanded during several stimulation cycles and frozen in aliquots that were freshly thawed before each use in an assay. Neuroblastoma cells were cocultured with HCMV pp65-specific $CD8^+$ T cells 4 to 5 hours in the presence of Golgistop (1/1,500; BD Biosciences). Cells were subsequently stained for surface markers and presence of intracellular IFNγ and TNF, followed by flow cytometry–based analysis.

Immunoblotting

Cells were lysed in sample buffer, separated by SDS-PAGE and transferred onto polyvinylidene fluoride (PVDF) membranes (Millipore) by wet immunoblotting. Membranes were blocked with 4% nonfat milk powder (Campina) in PBS 0.1% Tween-20 (Bio-Rad) for 1 hour and subsequently incubated with a primary antibody for 16 hours at 4°C. After washing, membranes were incubated with HRP-coupled secondary antibody for 1 hour followed by analysis on chemidoc imaging system (Bio-Rad).

Immunoprecipitation assay

Cells were lysed in PBS(1% CHAPS, 30 mmol/L Tris-HCL pH 8.0, 150 mmol/L NaCl) for 30 minutes on ice and spun down at $13{,}000 \times g$ for 15 minutes. Supernatants were incubated with uncoupled or antibody-coupled beads (Protein A-agarose beads, Roche) for 16 hours under constant agitation. Beads were separated from lysates by centrifugation, washed twice and resuspended in sample buffer. Protein interactions were analyzed using immunoblotting (see above).

Mass spectrometry

Immunoprecipitation beads were heated in sample loading buffer for 5 minutes. at 95°C, eluates were run into the stacking of a 4% to 12% Bis-Tris gel and coomassie-stained bands were excised. Proteins were reduced with 6.5 mmol/L DTT, alkylated with 54 mmol/L iodoacetamide and digested in-gel with trypsin (Gold, mass spectrometry grade, Promega, 3 ng/μL) overnight at 37°C. Extracted peptides were vacuum dried, reconstituded in 10% formic acid and analyzed by nanoLC-MS/MS on an Orbitrap Fusion Tribrid mass spectrometer equipped with a Proxeon nLC1000 system (Thermo Scientific). Peptides were loaded directly on the analytical column (Agilent Poroshell EC-C18 120 2.7 μm, 50 μm × 500 mm, packed in-house) and separated in a 140-minutes gradient containing a 124-minutes linear increase from 6% to 30% solvent B (0.1% formic acid/80% acetonitrile), with 0.1% formic acid/water as Solvent A. Further settings were as described previously (25).

Proteomic analysis

Raw data were analyzed by MaxQuant (version 1.5.8.3; ref. 26) using the label-free quantitation (LFQ) algorithm and the "match between runs" tool, with default settings. MS/MS data were searched against the human Swissprot database (20,197 entries, release 2016_09) complemented with a list of common contaminants and concatenated with the reversed version of all sequences. Trypsin/P was chosen as cleavage specificity allowing two missed cleavages. Carbamidomethylation (C) and oxidation (M) were set as fixed and variable modification, respectively. LFQ intensities were $\log_2$-transformed in Perseus (version 1.5.5.3; ref. 27), after which, proteins were filtered for at least two valid values (out of 3 total). Missing values were replaced by imputation based on a normal distribution using a width of 0.3 and a downshift of 1.8. P values of all quantified proteins were calculated in a Student t test and plotted against the $\log_2$ (bait/control) LFQ abundance difference in a Volcano plot. Proteins were considered enriched by immunoprecipitation when they met the criteria $P < 0.05$ and log2 LFQ[bait/control] ≥ 2.

Survival analysis

RNA seq dataset (GSE62564) was selected from the Gene Expression Omnibus and analyzed through the Genomics Analysis and Visualization Platform. Kaplan–Meier estimates of overall survival were determined using automatically generated expression cutoff values based on statistical significant differences using log-rank test.

Statistical analysis

All statistical analyses were performed using Graphpad Prism 7.02.

Results

Low expression of MHC-1 and NF-κB in neuroblastoma

Children of merely 3-months-old can present with neuroblastoma tumors, which advanced the idea that this type of tumor arises from erroneous embryonic development rather than external mutagenic factors. Therefore, considering the early developmental origins of these tumors, neuroblastoma might have originated from precursors that are yet to develop immunological features such as MHC-1, which is conceptionally different from tumors that downregulate MHC-1 as immune evasion strategy. To gain insight into MHC-1 gene expression and its regulation in neuroblastoma, we analyzed expression datasets of neuroblastoma tumors, healthy neural crest cells and healthy mature nerve tissue for MHC-1 and its transcription factors. Although MHC-1 expression in neuroblastoma was indeed lower than healthy mature nerve tissue, we found no differences in MHC-1 gene expression between neuroblastoma tumors and healthy neural crest cells (Fig. 1A). Neuroblastoma appears to reflect the underdeveloped state of the neural crest in which MHC-1 expression is still low, but can be evoked.

Downloaded from http://aacrjournals.org/cancerres/article-pdf/78/23/6621/2601371/6621.pdf by guest on 12 October 2024

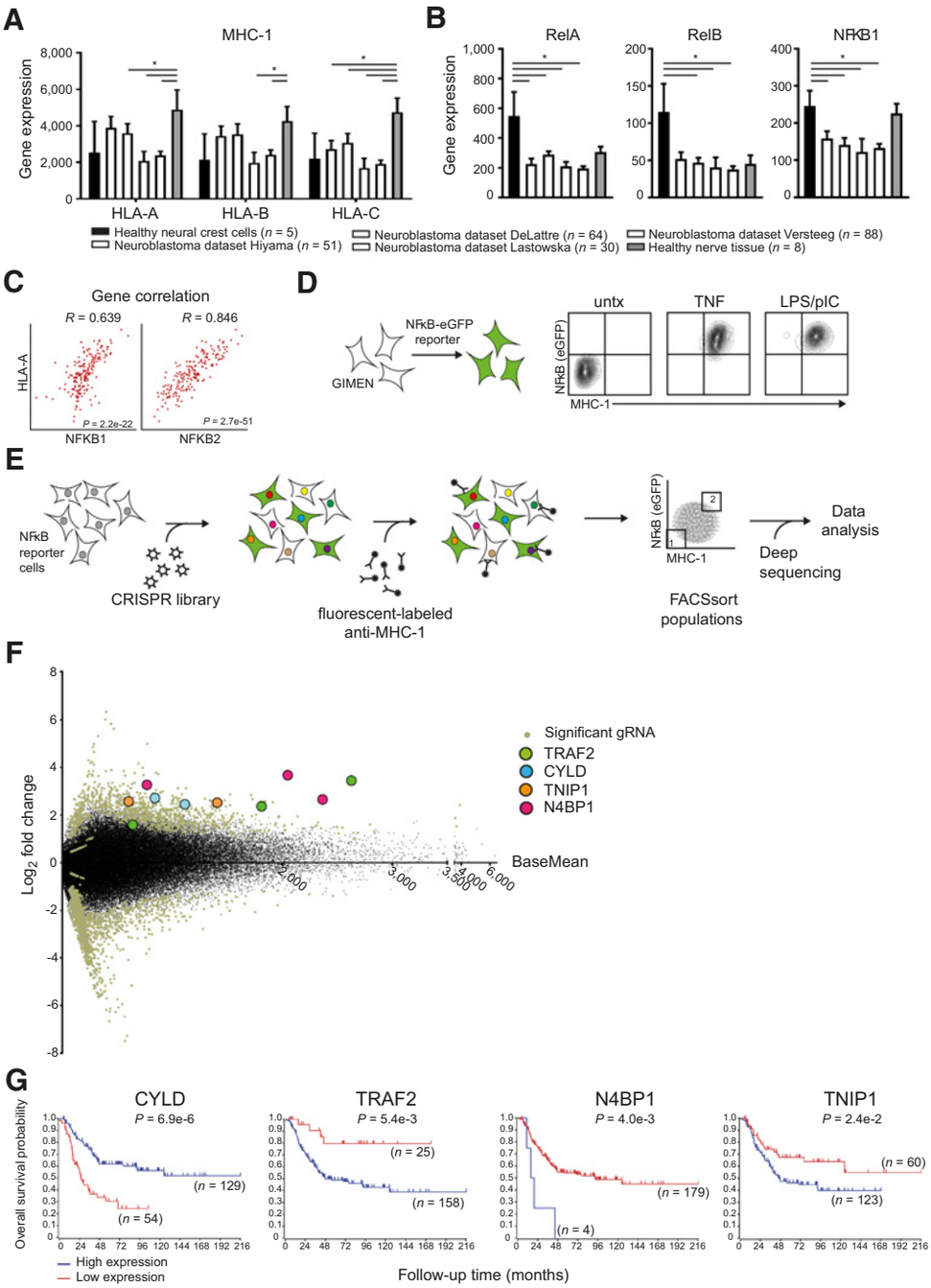

Figure 1.

Identification of NF-κB and MHC-1 suppressors in neuroblastoma. **A** and **B,** Gene-expression datasets of neural crest cells, healthy nerve tissue, and neuroblastoma tumors were analyzed for the expression of MHC-1 alleles HLA-A, HLA-B, and HLA-C (**A**) and NF-κB alleles RelA, RelB, and NFKB1 (**B**). Two-way ANOVA test was used. *, $P < 0.05$ was considered significant. **C,** Gene expression of HLA-A in neuroblastoma tumor samples (cohort of 183 patients with stage-4 neuroblastoma) was correlated with NFKB genes. Significance test for the Pearson correlation coefficient *r* was conducted. $P < 0.5$ was considered significant. **D,** Generation of an NF-κB reporter cell line. NF-κB activation and MHC-1 expression of the reporter cells was measured when untreated or after treatment with TNF or TLR ligands (LPS + polyI:C). **E,** Schematic overview of the performed screen. In short, neuroblastoma cells containing an NF-κB-eGFP reporter were subjected to a lentiviral CRISPR/Cas9 library. Cells were stained for MHC-1 using fluorescent-labeled antibodies and sorted by FACS. DNA was isolated from the collected populations and prepared for deep-sequencing to reveal the CRISPR content per population. **F,** CRISPR screen results are shown as $\log_2$-fold change of gRNAs in NFκB^{high}MHC^{high} population versus NF-κB^{low}MHC^{low} population. The BaseMean, the mean of the normalized guide counts of the four samples, is plotted on the *x*-axis. Significant gRNAs are highlighted in gray and significant gene hits, with a BaseMean of >500 reads, are depicted as circles. Screen results are based on two independent replicates. See Supplementary Fig. S2 for more information about the replicates. **G,** In a cohort of 183 patients with stage-4 neuroblastoma, the expression levels of NF-κB suppressors CYLD, N4BP1, TNIP1, and TRAF2 were correlated with survival data. Log-rank test was used, $P < 0.05$ was considered significant.

Downloaded from http://aacrjournals.org/cancerres/article-pdf/78/23/6621/2601371/6621.pdf by guest on 12 October 2024

Transcriptional control of MHC-1 is well understood as various transcription factors have been identified that establish MHC-1 in human cells, including NF-κB, NLRC5 and IRF1. Overall, these MHC-1 transcription factors were not highly expressed in neuroblastoma (Fig. 1B; Supplementary Fig. S1). NLRC5 and IRF1 were not highly expressed in neural crest cells either, as we found similar expression levels between neuroblastoma tumors and neural crest cells (Supplementary Fig. S1). In contrast, gene expression of multiple NF-κB family members (RelA, RelB, NFKB1, NFKB2, and Rel) was higher in neural crest cells than in neuroblastoma tumors. In particular, expression of RelA, RelB, and NFKB1 was significantly decreased in neuroblastoma tumors (Fig. 1B). Also compared with mature nerve tissue, RelA and NFKB1 expression was reduced. As neural crest cells differentiate toward mature nerve cells, the MHC-1 locus becomes available for transcription causing the developmental upregulation of MHC-1. Although in healthy cells NF-κB expression stimulates *de novo* MHC-1 transcription, in neuroblastoma NF-κB expression is suppressed causing a lack in the normal developmental MHC-1 upregulation. Gene expression of MHC-1 alleles correlated with NFKB gene expression in stage-4 neuroblastoma tumors (Fig. 1C; Supplementary Fig. S1), indicating that MHC-1 expression can be increased in neuroblastoma by NF-κB. Of note, NF-κB family member Rel was upregulated in neuroblastoma, which is in agreement with its role in antiapoptotic signaling (28, 29).

Thus, the abnormal development from healthy neural crest cell to malignant neuroblastoma coincides with downregulation of NF-κB family members. In line with this observation, several studies have shown that transcriptional activity of NF-κB in neuroblastoma cells is indeed repressed (13, 14, 17). These data together support that reversal of repressed NF-κB might steer neuroblastoma away from tumorigenic development and possibly unlock MHC-1 expression for immunogenic display.

Identification of NF-κB–dependent MHC-1 suppressors in neuroblastoma

NF-κB is repressed in neuroblastoma on both gene expression level (Fig. 1B) as well as activation level (13, 14, 17). Activation of NF-κB can temporarily restore MHC-1 expression in neuroblastoma, suggesting that NF-κB signaling is repressed by unknown mechanisms, leading to low immunogenicity of neuroblastoma tumors. To establish stable MHC-1 expression in neuroblastoma, we set out to identify the factors that negatively regulate NF-κB–mediated MHC-1 expression in neuroblastoma.

To this end, we generated a clonal cell line bearing an NF-κB reporter, which upon activation of the NF-κB pathway expresses eGFP (Fig. 1D). Indeed, elevated MHC-1 levels were observed upon stimulation of the NF-κB pathway using TNF or TLR ligands. These cells were mutagenized using a genome-wide CRISPR/Cas9 knockout library containing 118.000 individual gRNAs with an average of 6 gRNAs per gene (30). The mutagenized cells were expanded and stained for cell surface expression of MHC-1. NF-κB^{neg}MHC^{neg} and NF-κB^{pos}MHC^{pos} populations were isolated using FACSsorting. Next-generation sequencing was used to identify gRNAs enriched for each population (Fig. 1E).

Each individual gRNA was traced back and scored for its enrichment in either the NF-κB^{neg}MHC^{neg} or the NF-κB^{pos}MHC^{pos} population (Fig. 1F; Supplementary Fig. S2). As 6 different gRNAs were used per gene, the scores of all 6 gene-specific gRNAs combined were used to calculate significant gene hits. This resulted in a total of 9 genes that were identified as candidate regulators of NF-κB activity and MHC-1 expression in neuroblastoma cells (Supplementary Table S1), including 4 positive regulators and 5 suppressors. We selected Nedd4-binding protein 1 (N4BP1), TNFAIP3-interacting protein 1 (TNIP1), cylindromatosis (CYLD), and TNF-receptor–associated factor 2 (TRAF2) as candidate suppressors of NF-κB and MHC-1 in neuroblastoma cells shown in Fig. 1F (See Materials and Methods for selection criteria). The expression of N4BP1, TNIP1, and TRAF2, but not CYLD, correlated with worse survival in patients with stage-4 neuroblastoma (Fig. 1G), suggesting an important role for NF-κB suppression in malicious outcome of neuroblastoma.

CYLD and TRAF2 are well-established regulators of NF-κB signaling. Whereas CYLD inhibits NF-κB upon receptor signaling (31, 32), TRAF2 maintains an inactive NF-κB in steady-state conditions (33), but not upon signaling. Furthermore, the inhibitory effect of TNIP1 on NF-κB is shown to impede canonical NF-κB (34, 35). Moreover, N4BP1 has been implicated in NF-κB inhibition (36); however, the mechanism remains elusive.

These results suggest that upon depletion of N4BP1 or TNIP1, NF-κB^{neg}MHC^{neg} neuroblastoma cells transform into cells endowed with stable expression of MHC-1 and an active NF-κB transcription factor.

Depletion of NF-κB suppressors enhances MHC-1 in neuroblastoma

Using CRISPR/Cas9, we generated N4BP1- and TNIP1-depleted neuroblastoma reporter clones and empty vector-transduced wild type (WT) reporter cells as controls (Supplementary Fig. S3). NF-κB activity and MHC-1 expression were measured by flow cytometry. Depletion of N4BP1 or TNIP1 resulted in activation of the NF-κB reporter (Fig. 2A). Activation of NF-κB was also shown by confocal microscopy of WT and ΔN4BP1 and ΔTNIP1 neuroblastoma cells (Fig. 2B). Total RelA protein localized to the cytosol in WT cells, but spontaneously translocated to the nucleus in ΔN4BP1 and ΔTNIP1 cells. Nuclear translocation requires phosphorylation of RelA protein, indeed, phospho-RelA was only detected in ΔN4BP1 and ΔTNIP1 cells and not WT neuroblastoma cells. In addition, ΔN4BP1 and ΔTNIP1 cells showed increased surface levels of MHC-1 compared with WT cells (Fig. 2C), corroborating the findings of the CRISPR screen. Moreover, inversed correlation between N4BP1 and MHC-1 gene expression could be observed in 46 patients (Supplementary Fig. S4) and associated with a significant difference in survival probability, with high expression of N4BP1 relating to worse survival (Fig. 2D). For 42 patients an inversed correlation between TNIP1 and MHC-1 gene expression was observed, which also resulted in worse survival for TNIP1^{high}-expressing tumors.

To investigate whether the inhibitory effects of N4BP1 and TNIP1 on NF-κB and MHC-1 are specific for neuroblastoma, we generated a panel of N4BP1 and TNIP1 mutants in a range of human cell lines (Supplementary Fig. S5). MHC-1 expression levels were measured in WT and knockout cells using flow cytometry (Fig. 2C). Depletion of N4BP1 or TNIP1 generally resulted in increased MHC-1 membrane expression across five neuroblastoma cell lines. Differences in gene expression of either HLA-A or HLA-B genes were measured using qPCR (Fig. 2E). Interestingly, in non-neuroblastoma cell lines HEK293T and BLM, MHC-1 upregulation was not clearly different between WT

Downloaded from http://aacrjournals.org/cancerres/article-pdf/78/23/6621/2601371/6621.pdf by guest on 12 October 2024

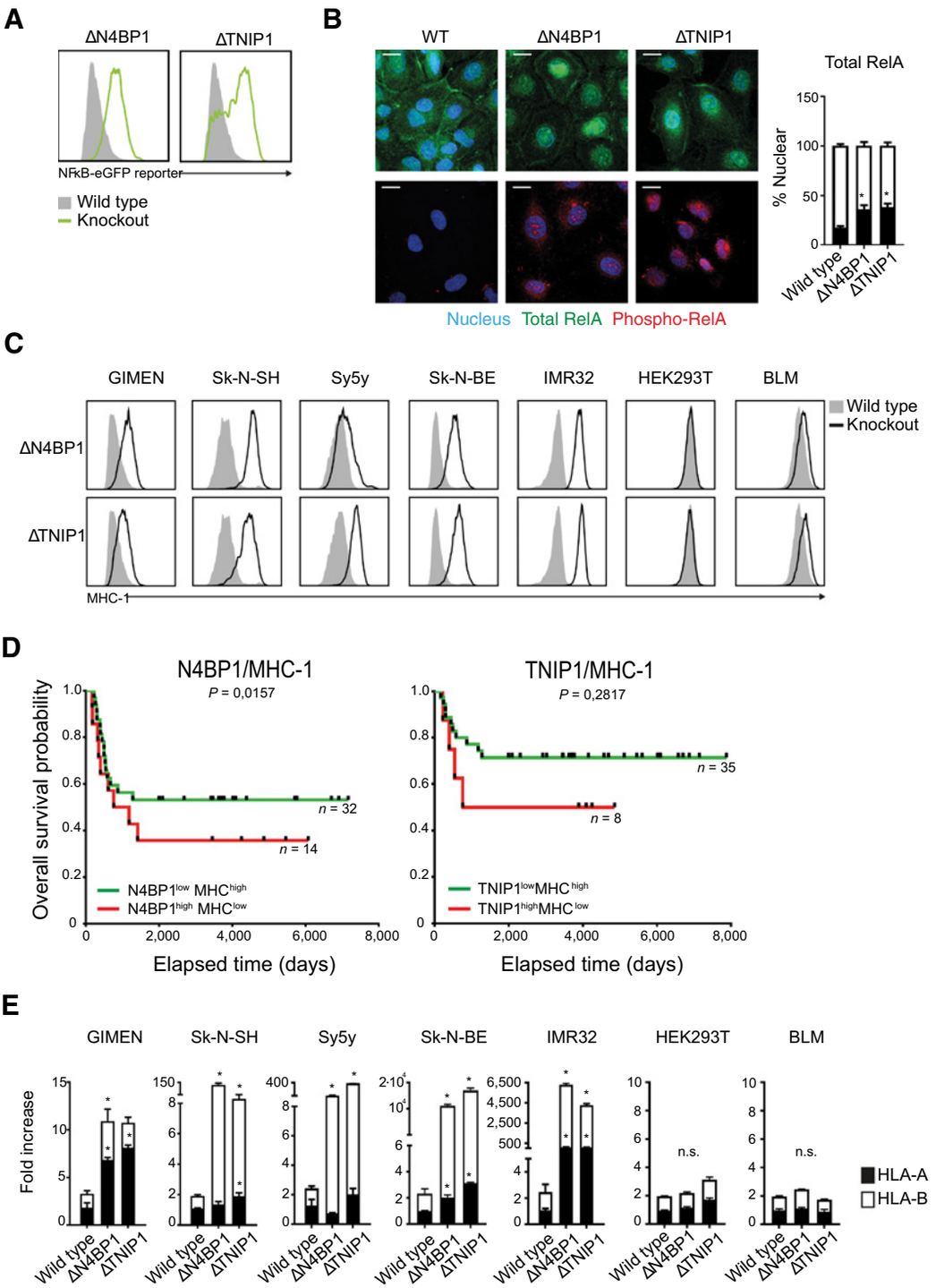

Figure 2.

Effect of N4BP1 and TNIP1 depletion on NF-κB and MHC-1 across cell lines. **A,** The eGFP fluorescence produced by NF-κB reporter activity was measured in single-cell clones of ΔN4BP1 and ΔTNIP1 neuroblastoma GIMEN cells compared with WT (empty vector control). **B,** Left, confocal images of WT, ΔN4BP1, and ΔTNIP1 neuroblastoma GIMEN cells stained for total RelA protein (green) and phospho-RelA protein (red). Nuclei, blue. Scale bar, 10 μm. Right, quantification of nuclear localization of RelA protein. **C,** N4BP1 or TNIP1 was depleted in indicated cell lines and surface expression of MHC-1 was measured by flow cytometry. **D,** Survival probability for patient groups with neuroblastoma tumors showing inversed correlated N4BP1/MHC-1 expression (left) or TNIP1/MHC-1 expression (right). **E,** Relative gene expression of MHC-1 alleles HLA-A and HLA-B was measured by qPCR in WT, ΔN4BP1, and ΔTNIP1 cells. Fold increase of HLA-A expression (black) or HLA-B expression (white) in knockout cells compared with WT cells is depicted in the graphs. Mann–Whitney *U* tests were used. *, $P < 0.05$ was considered significant; n.s., nonsignificant.

Downloaded from http://aacrjournals.org/cancerres/article-pdf/78/23/6621/2601371/6621.pdf by guest on 12 October 2024

and knockout cells, suggesting that the high steady-state expression levels of MHC-1 in HEK293T and BLM make them less prone for increased MHC-1 expression. However, immunoblot analysis of ΔN4BP1 and ΔTNIP1 cells of HEK293T and BLM shows increased levels of phospho-RelA, indicating that NF-κB is activated (Supplementary Fig. S6). These results suggest that NF-κB inhibition by N4BP1 and TNIP1 is conserved across multiple cell types, but its effect on MHC-1 levels is cell-type specific.

Antitumor T-cell reactivity against NF-κB–active neuroblastoma cells

Expression of peptide/MHC-1 complexes on the neuroblastoma cell surface is essential to T-cell recognition and possible T-cell–based immunotherapy (13, 19, 20). We next addressed whether increased MHC-1 expression in ΔN4BP1 and ΔTNIP1 neuroblastoma cells is sufficient to trigger functional antigen presentation and T-cell reactivity. results in functional antigen presentation and T-cell reactivity, and therefore performed co-culture experiments using neuroblastoma cells and MHC-matched antigen-specific CTLs. To test this, we generated WT and knockout neuroblastoma cells that stably express the model antigen pp65, and exposed these cells to MHC-1–restricted pp65-specific CTLs in coculture experiments. We found that although CTLs were activated upon coculture with ΔN4BP1 or ΔTNIP1 cells, WT cells failed to do so (Fig. 3A). Indicative of T-cell activation and granule release, the CTLs produced IFNγ and showed LAMP1 surface staining, respectively.

Demethylating agent decitabine (DAC) has been shown to increase MHC-1 expression and is currently being scrutinized in several clinical trials for patients with neuroblastoma (37–39). Treatment with decitabine indeed increased MHC-1 levels on neuroblastoma cells to a similar extent as ΔN4BP1/TNIP1 depletion (Fig. 3B). The combination of DNA demethylation with active NF-κB transcription shows a 2-fold higher induction of MHC-1 surface expression. Such a synergistic effect is also observed when testing the T-cell reactivity against decitabine-treated knockout cells. T-cell recognition of ΔN4BP1 and ΔTNIP1 cells increased by 7-fold and 5-fold, respectively, when treated with decitabine (Fig. 3A). Thus, active NF-κB makes neuroblastoma cells immunogenic for T-cell reactivity. These results highlight the significance of NF-κB modulation for anti-neuroblastoma immunotherapies, alone or as adjuvant treatment to currently tested protocols.

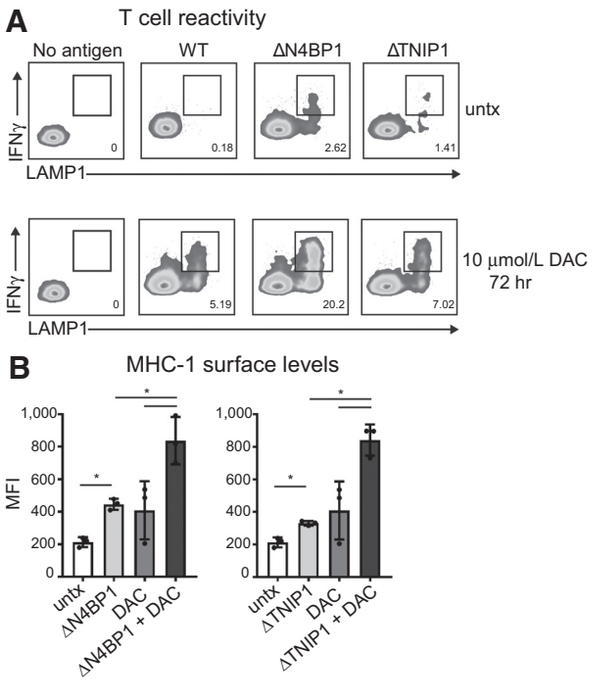

Figure 3.

$CD8^+$ T-cell recognition of ΔN4BP1 and ΔTNIP1 neuroblastoma cells. WT, ΔN4BP1, and ΔTNIP1 neuroblastoma GIMEN cells stably expressing pp65 model antigen were left untreated or were treated with decitabine for 72 hours. **A,** After coculture with pp65-specific $CD8^+$ T cells in a 1:1 ratio, T cells were stained for surface LAMP1 expression and intracellular production of IFNγ and analyzed by flow cytometry. Neuroblastoma cells lacking pp65 expression were used as negative control. **B,** Membrane MHC-1 expression levels were measured by flow cytometry. Mann–Whitney *U* tests were used. *, $P < 0.05$ was considered significant. MFI, mean fluorescence intensity.

Differential NF-κB activation in ΔN4BP1 and ΔTNIP1 cells

TNIP1 modulates NF-κB activity by destabilizing the IKK complex (40) with a consequential sequestering of RelA by IκB, less nuclear translocation and diminished transcription of target genes including MHC-1. How N4BP1 modulates NF-κB activity remains unclear. To investigate which NF-κB members play a role in ΔN4BP1 cells, we looked at the expression levels of the five transcriptionally active subunits (phospho-RelA, RelB, p50, p52, and c-Rel) of NF-κB by immunoblot. Compared with WT, ΔN4BP1 cells showed increased levels of phosphorylated RelA, of RelB and p52 (Fig. 4A). This is different from ΔTNIP1 cells that only showed increases in p-RelA and RelB, but no effects on the other subunits. Next, we tested whether these subunits also contribute to NF-κB-mediated gene expression by disrupting each subunit in the ΔN4BP1 or ΔTNIP1 neuroblastoma reporter cells using CRISPR/Cas9. We designed gRNAs against the NF-κB genes RelA, RelB, NFKB1 and NFKB2 and used these to transduce WT, ΔN4BP1 and ΔTNIP1 cells. NF-κB reporter activity was measured seven days after transduction. In ΔN4BP1 cells, NF-κB reporter activity was decreased when RelA or NFKB2 (= p52) was depleted (Fig. 4B). In ΔTNIP1 cells, NF-κB reporter activity was decreased only when RelA was depleted. In contrast, RelB depletion did not affect reporter activity in either ΔN4BP1 or ΔTNIP1 cells, despite increased RelB expression.

Thus, although N4BP1 and TNIP1 both inhibit NF-κB activity, they appear to do so using different mechanisms. In ΔN4BP1 cells both RelA and p52 contribute to NF-κB-mediated gene transcription, indicating that N4BP1 inhibition broadly affects both canonical and noncanoncial NF-κB subunits. In ΔTNIP1 cells on the other hand, only canonical RelA appears to be the driver of NF-κB-mediated gene activation.

N4BP1 coordinates degradation of NF-κB–initiating kinase NIK

To gain more insight into the mechanism by which N4BP1 inhibits both p-RelA and p52, we decided to seek out the binding partners of N4BP1. To this end, a protein-protein interaction experiment was performed combining antibody-mediated pull-down with mass spectrometry. WT neuroblastoma cells were transfected with His-tagged N4BP1-expressing constructs and after 48 hours lysed for coimmunoprecipitation experiments

Downloaded from http://aacrjournals.org/cancerres/article-pdf/78/23/6621/2601371/6621.pdf by guest on 12 October 2024

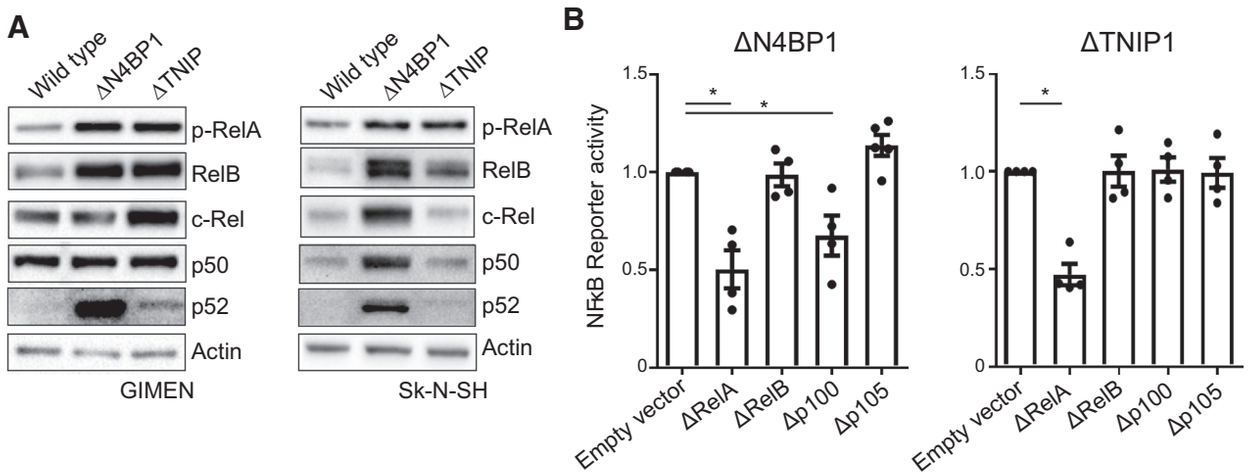

Figure 4.

Contribution of NF-κB family members to increased NF-κB activity in ΔN4BP1 and ΔTNIP1 neuroblastoma cells. **A,** Immunoblot analysis of phospho-RelA, RelB, c-Rel, p50 (cleaved from p105) and p52 (cleaved from p100) in WT, ΔN4BP1, and ΔTNIP1 cells. **B,** Genes encoding RelA, RelB, p105 (NFKB1) and p100 (NFKB2) were depleted in ΔN4BP1 and ΔTNIP1 neuroblastoma GIMEN cells using the CRISPR/Cas9 lentiviral construct. An empty vector construct was used as negative control. After a week, cells were collected and NF-κB-eGFP reporter signal was measured by flow cytometry. One-way ANOVA tests were used. *, $P < 0.05$ was considered significant.

using anti-His beads. Mass spectrometry was used to identify proteins bound to N4BP1-His.

A variety of binding partners of N4BP1 were identified and among them, one in particular caught our attention. The de-ubiquinating enzyme CEZANNE was significantly enriched in N4BP1-His coimmunoprecipitates (Fig. 5A). As observed for N4BP1, also CEZANNE expression levels correlated with worse survival in patients with stage-4 neuroblastoma (Fig. 5B). Mechanistically, CEZANNE stabilizes TRAF3 by removing TRAF3-bound ubiquitin modifications, thereby controlling NF-κB activation (41). Stabilized TRAF3 takes part in a protein complex that retains NIK and facilitates ubiquitination and degradation of NIK. Conversely, the degradation of TRAF3 causes NIK to accumulate and phosphorylate down-stream targets thereby initiating p100 cleavage into p52 and activation of noncanonical NF-κB. In addition, TRAF3 degradation

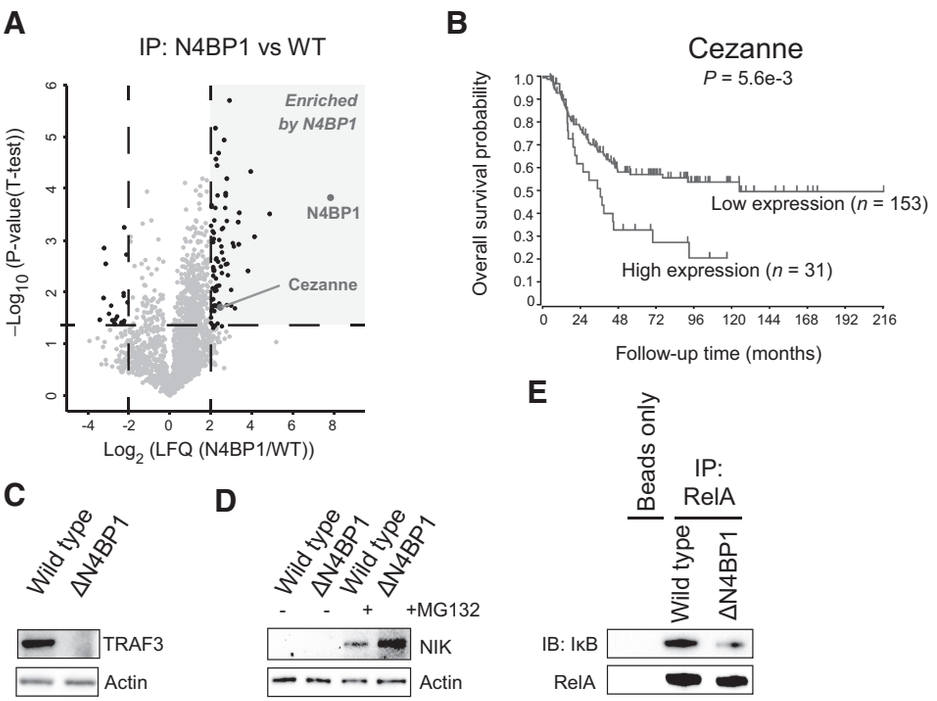

Figure 5.

N4BP1 inhibits both canonical and noncanonical NF-κB through CEZANNE. **A,** Identification of possible binding partners of N4BP1. WT neuroblastoma cells were transfected with N4BP1-His6 or left untreated. After 48 hours, cells were lysed and proteins were immunoprecipitated using anti–HIS-beads. Immunoprecipitates were analyzed by mass spectrometry. **B,** In a cohort of 183 patients with stage-4 neuroblastoma, the expression levels of Cezanne were correlated with survival data. Log-rank test was used. $P < 0.05$ was considered significant. **C,** Immunoblot analysis of TRAF3 in WT and ΔN4BP1 cells. **D,** Immunoblot analysis of NIK in WT and ΔN4BP1 cells treated with proteasome inhibitor MG132. **E,** The amount of sequestered RelA protein in WT and ΔN4BP1 cells. Total RelA protein of WT and ΔN4BP1 cells was immunoprecipitated using beads and analyzed for presence of IκB protein.

Downloaded from http://aacrjournals.org/cancerres/article-pdf/78/23/6621/2601371/6621.pdf by guest on 12 October 2024

was shown to also activate the canonical pathway involving RelA (42).

To confirm that N4BP1 is involved in stabilizing TRAF3 and break-down of NIK, the protein levels of TRAF3 and NIK were measured in WT and ΔN4BP1 cells using immunoblot (Fig. 5C and D). In ΔN4BP1 cells, we detected decreased levels of TRAF3 protein compared with WT cells, suggesting that TRAF3 is degraded when N4BP1 is absent. In addition, higher levels of NIK kinase are detected in ΔN4BP1 cells compared with WT cells, indicating that NIK accumulates in absence of N4BP1. Given that TRAF3 degradation and subsequent NIK accumulation leads to processing of p100 into p52, these results could explain the spontaneous activation of noncanonical NF-κB in ΔN4BP1 neuroblastoma cells.

TRAF3 was shown to also control the canonical pathway through attenuating phosphorylation and degradation of the Inhibitor of NF-κB (IκB; ref. 42) and keeping RelA protein sequestered. Therefore, to determine a possible role of IκB in ΔN4BP1 cells, we measured the levels of IκB bound to RelA using immunoprecipitation followed by immunoblot (Fig. 5E). We found that RelA was in reduced amounts complexed with IκB in ΔN4BP1 cells, rendering RelA free for activation. In contrast, in WT cells, IκB was clearly bound to RelA, indicating sequestering and inhibition of RelA and canonical NF-κB.

Thus, N4BP1 functions as a negative regulator of the NF-κB pathway in neuroblastoma, as contributed by both the canonical and noncanonical branches, where N4BP1 uses CEZANNE to stabilize TRAF3, resulting in degradation of NIK and sequestering of RelA by IκB. Upon depletion of N4BP1, TRAF3 is degraded, NIK levels accumulate and IκB detaches from RelA for ensued signaling to target genes, including MHC-1.

Discussion

In this study, we investigated the repressed NF-κB–mediated MHC-1 expression in neuroblastoma. We show that gene expression levels of NF-κB members are actively repressed during tumorigenic development of neural crest cells toward neuroblastoma tumor cells. Repression of NF-κB proteins in neuroblastoma has been reported previously (13, 17). Van `t Veer and colleagues (14) use neuroblastoma rat cell lines to show decreased expression of p105/p50 protein and regulation thereof by the oncogene NMYC. In contrast, a study in human neuroblastoma cell lines shows low transcriptional availability of NF-κB in neuroblastoma in an NMYC-independent manner (17). In support of the latter study, the performed CRISPR/Cas9 knockout screen we describe here also did not identify NMYC as a negative regulator of NF-κB. However, our screen results were not saturated due to technical restraints therefore a role for NMYC in NF-κB inhibition in neuroblastoma remains plausible. Of note, the p105/p50 subunit did not contribute to NF-κB activity in ΔN4BP1 or ΔTNIP1 neuroblastoma cells, indicating that N4BP1 or TNIP1 do not use NMYC-p50 regulation for NF-κB inhibition.

Nevertheless, restoration of canonical NF-κB can increase MHC-1 expression in neuroblastoma (13, 14, 17). Transfection of NMYC-amplified cells with a p50-expressing construct showed MHC-1 expression (14). Moreover, transfection of RelA increased MHC-1 membrane levels in neuroblastoma (13, 17). Combined activation of NF-κB and the IRF1 transcription factor further increased MHC-1 expression (13), however we have no indication that IRF1 is involved in MHC-1 upregulation observed in ΔN4BP1 or ΔTNIP1 neuroblastoma cells (Supplementary Fig. S7). In ΔN4BP1 and ΔTNIP1 cells we clearly observe activation of canonical NF-κB as RelA is dissociated from IκB protein and highly phosphorylated. In addition, in ΔN4BP1 cells we also observe activation of noncanonical NF-κB involving the RelB and p100/p52 proteins.

N4BP1 was first described as an inhibitor of the E3 ligase Itch thereby stabilizing cell death regulators such as p73α and c-Jun (43). In 2009, N4BP1 was implicated in NF-κB regulation by Fenner and colleagues (44). In a coimmunoprecipitation experiment using polyubiquitin, N4BP1 and other proteins were isolated. A number of these ubiquitin-binding proteins were revealed as negative regulators of NF-κB. Although N4BP1 was not followed-up in this study, its ubiquitin-binding capacity implicated the possibility for regulating NF-κB. Then, in 2011 a direct role of N4BP1 in controlling NF-κB activity was first observed (36). Through overexpression in NF-κB reporter cells, N4BP1 was found as the most effective negative regulator of NF-κB. We here extend the knowledge about N4BP1 as an NF-κB suppressor by showing its interaction with deubiquitinating enzyme CEZANNE. CEZANNE regulates TRAF3 levels (41), by which it controls both canonical and noncanonical NF-κB (42). As such, N4BP1 prevents NF-κB activation by orchestrating CEZANNE-mediated deubiquitination of TRAF3 thereby stabilizing TRAF3 protein. Intact TRAF3 results in constant degradation of NIK and thus obstruction of noncanonical NF-κB activation. Also, RelA protein was sequestered by IκB when TRAF3 was present, leading to inhibition of canonical NF-κB.

The NF-κB suppressors N4BP1, CEZANNE, and TNIP1 independently correlate with worse survival in patients with stage-4 neuroblastoma. Despite the clear role shown here of NF-κB suppressors preventing T-cell recognition, there is yet no evidence for an immunological reason underpinning this difference in survival. Since low expression of NF-κB suppressors did not prevent neuroblastoma development, a survival difference might be explained by predisposition of the tumor for post-treatment immune responses. One possibility is that after stem cell transplantation of patients with neuroblastoma, newly developing immune cells can eliminate residing tumor cells that express low levels of NF-κB suppressors better than tumor cells that express high levels of NF-κB suppressors, which would result in better clearance of NF-κB–active neuroblastomas. Alternatively, low expression of NF-κB suppressors may render neuroblastoma tumors more sensitive for current treatment. For example, NF-κB activation is required for certain cytotoxic agents to kill neuroblastoma cells (45, 46). Also, efficacy of retinoic acid-induced differentiation of neuroblastoma cells requires an active NF-κB pathway (47–49).

Taken together, we have uncovered that aberrant NF-κB functioning in neuroblastoma results in decreased MHC-1 expression, escape from T-cell immune surveillance and poor survival in stage-4 patients. The strategy chosen here, combining an NF-κB reporter and MHC-1 cell surface staining in combination with a genome-wide CRISPR/Cas9 library, has to our knowledge not been performed before. The identification of novel and previously identified members of the NF-κB signaling pathway illustrates that this strategy has been successful. A limitation to our study is that several described NF-κB and MHC-1 regulators were not retrieved using this method. A possible explanation for this is the quality of this early generation CRIPSR/Cas9 library requires further optimization. A library

Downloaded from http://aacrjournals.org/cancerres/article-pdf/78/23/6621/2601371/6621.pdf by guest on 12 October 2024

containing more, and better validated, gRNAs targeting each gene could lead to a better separation of mutants. Nevertheless, we have identified NF-κB suppressors that may serve as drug targets to increase neuroblastoma immunogenicity, which is necessary for immunotherapies to translate into clinical benefits for patients with stage-4 neuroblastoma.

Disclosure of Potential Conflicts of Interest

T.R. Brummelkamp has ownership interest (including stock, patents, etc.) in Scenic Biotech and Haplogen. No potential conflicts of interest were disclosed by the other authors.

Authors' Contributions

Conception and design: L. Spel, J. Nieuwenhuis, S. Nierkens, M. Boes
Development of methodology: L. Spel, J. Nieuwenhuis, S. Nierkens, M. Boes
Acquisition of data (provided animals, acquired and managed patients, provided facilities, etc.): L. Spel, J. Nieuwenhuis, R. Haarsma, O.B. Bleijerveld, M. Altelaar, T.R. Brummelkamp, S. Nierkens
Analysis and interpretation of data (e.g., statistical analysis, biostatistics, computational analysis): L. Spel, J. Nieuwenhuis, R. Haarsma, E. Stickel, O.B. Bleijerveld, M. Altelaar, T.R. Brummelkamp, S. Nierkens, M. Boes
Writing, review, and/or revision of the manuscript: L. Spel, J. Nieuwenhuis, R. Haarsma, E. Stickel, J.J. Boelens, S. Nierkens, M. Boes
Administrative, technical, or material support (i.e., reporting or organizing data, constructing databases): L. Spel, S. Nierkens
Study supervision: J.J. Boelens, S. Nierkens, M. Boes

Acknowledgments

We thank J.E. Carette for kindly providing us with the NF-κB reporter plasmid. This work was supported by the Villa Joep Foundation and the Netherlands Organization for Scientific Research (NWO), as part of the National Roadmap Large-scale Research Facilities of the Netherlands, Proteins@Work (project number 184.032.201). S. Nierkens and J.J. Boelens received funding from The Villa Joep Foundation and AMMODO. O.B. Bleijerveld and M. Altelaar received funding from Dutch Scientific Research (NWO), as part of the National Roadmap Large-scale Research Facilities of the Netherlands.

The costs of publication of this article were defrayed in part by the payment of page charges. This article must therefore be hereby marked *advertisement* in accordance with 18 U.S.C. Section 1734 solely to indicate this fact.

Received February 19, 2018; revised June 20, 2018; accepted September 10, 2018; published first September 13, 2018.

References

1. Davidoff AM. Neuroblastoma. Semin Pediatr Surg 2012;21:2–14.
2. Maris JM. Recent advances in neuroblastoma. N Engl J Med 2010;362:2202–11.
3. Louis CU, Shohet JM. Neuroblastoma: molecular pathogenesis and therapy. Annu Rev Med 2015;66:49–63.
4. Cheung NK, Dyer MA. Neuroblastoma: developmental biology, cancer genomics and immunotherapy. Nat Rev Cancer 2013;13:397–411.
5. Schumacher TN, Schreiber RD. Neoantigens in cancer immunotherapy. Science 2015;348:69–74.
6. Oberthuer A, Hero B, Spitz R, Berthold F, Fischer M. The tumor-associated antigen PRAME is universally expressed in high-stage neuroblastoma and associated with poor outcome. Clin Cancer Res 2004;10:4307–13.
7. Wolfl M, Jungbluth AA, Garrido F, Cabrera T, Meyen-Southard S, Spitz R, et al. Expression of MHC class I, MHC class II, and cancer germline antigens in neuroblastoma. Cancer Immunol Immunother 2005;54:400–6.
8. Jacobs JF, Brasseur F, Hulsbergen-van de Kaa CA, van de Rakt MW, Figdor CG, Adema GJ, et al. Cancer-germline gene expression in pediatric solid tumors using quantitative real-time PCR. Int J Cancer 2007;120:67–74.
9. Croce M, Corrias MV, Rigo V, Ferrini S. New immunotherapeutic strategies for the treatment of neuroblastoma. Immunotherapy 2015;7:285–300.
10. Seeger RC. Immunology and immunotherapy of neuroblastoma. Semin Cancer Biol 2011;21:229–37.
11. Raffaghello L, Prigione I, Airoldi I, Camoriano M, Morandi F, Bocca P, et al. Mechanisms of immune evasion of human neuroblastoma. Cancer Lett 2005;228:155–61.
12. Coughlin CM, Fleming MD, Carroll RG, Pawel BR, Hogarty MD, Shan X, et al. Immunosurveillance and survivin-specific T-cell immunity in children with high-risk neuroblastoma. J Clin Oncol 2006;24:5725–34.
13. Lorenzi S, Forloni M, Cifaldi L, Antonucci C, Citti A, Boldrini R, et al. IRF1 and NF-kB restore MHC class I-restricted tumor antigen processing and presentation to cytotoxic T cells in aggressive neuroblastoma. PLoS ONE 2012;7:e46928.
14. van't Veer LJ, Beijersbergen RL, Bernards R. N-myc suppresses major histocompatibility complex class I gene expression through down-regulation of the p50 subunit of NF-kappa B. EMBO J 1993;12:195–200.
15. Chaturvedi MM, Sung B, Yadav VR, Kannappan R, Aggarwal BB. NF-kappaB addiction and its role in cancer: `one size does not fit all'. Oncogene 2011;30:1615–30.
16. Lv D, Shen Y, Peng Y, Liu J, Miao F, Zhang J. Neuronal MHC class I expression is regulated by activity driven calcium signaling. PLoS ONE 2015;10:e0135223.
17. Forloni M, Albini S, Limongi MZ, Cifaldi L, Boldrini R, Nicotra MR, et al. NF-kappaB, and not MYCN, regulates MHC class I and endoplasmic reticulum aminopeptidases in human neuroblastoma cells. Cancer Res 2010;70:916–24.
18. Bao L, Dunham K, Lucas K. MAGE-A1, MAGE-A3, and NY-ESO-1 can be upregulated on neuroblastoma cells to facilitate cytotoxic T lymphocyte-mediated tumor cell killing. Cancer Immunol Immunother 2011;60:1299–307.
19. Vertuani S, De Geer A, Levitsky V, Kogner P, Kiessling R, Levitskaya J. Retinoids act as multistep modulators of the major histocompatibility class I presentation pathway and sensitize neuroblastomas to cytotoxic lymphocytes. Cancer Res 2003;63:8006–13.
20. Spel L, Boelens JJ, van der Steen DM, Blokland NJ, van Noesel MM, Molenaar JJ, et al. Natural killer cells facilitate PRAME-specific T-cell reactivity against neuroblastoma. Oncotarget 2015;6:35770–81.
21. Lee CC, Carette JE, Brummelkamp TR, Ploegh HL. A reporter screen in a human haploid cell line identifies CYLD as a constitutive inhibitor of NF-kappaB. PLoS One 2013;8:e70339.
22. Brinkman EK, Chen T, Amendola M, van Steensel B. Easy quantitative assessment of genome editing by sequence trace decomposition. Nucleic Acids Res 2014;42:e168.
23. Langmead B, Trapnell C, Pop M, Salzberg SL. Ultrafast and memory-efficient alignment of short DNA sequences to the human genome. Genome Biol 2009;10:R25.
24. Love MI, Huber W, Anders S. Moderated estimation of fold change and dispersion for RNA-seq data with DESeq2. Genome Biol 2014;15:550.
25. Ameziane N, May P, Haitjema A, van de Vrugt HJ, van Rossum-Fikkert SE, Ristic D, et al. A novel Fanconi anaemia subtype associated with a dominant-negative mutation in RAD51. Nat Commun 2015;6:8829.
26. Cox J, Hein MY, Luber CA, Paron I, Nagaraj N, Mann M. Accurate proteome-wide label-free quantification by delayed normalization and maximal peptide ratio extraction, termed MaxLFQ. Mol Cell Proteomics 2014;13:2513–26.
27. Tyanova S, Temu T, Sinitcyn P, Carlson A, Hein MY, Geiger T, et al. The Perseus computational platform for comprehensive analysis of (prote) omics data. Nat Methods 2016;13:731–40.
28. Gilmore TD, Gerondakis S. The c-Rel transcription factor in development and disease. Genes Cancer 2011;2:695–711.
29. Hunter JE, Leslie J, Perkins ND. c-Rel and its many roles in cancer: an old story with new twists. Br J Cancer 2016;114:1–6.
30. Sanjana NE, Shalem O, Zhang F. Improved vectors and genome-wide libraries for CRISPR screening. Nat Methods 2014;11:783–784.

Downloaded from http://aacrjournals.org/cancerres/article-pdf/78/23/6621/2601371/6621.pdf by guest on 12 October 2024

31. Kovalenko A, Chable-Bessia C, Cantarella G, Israel A, Wallach D, Courtois G. The tumour suppressor CYLD negatively regulates NF-kappaB signalling by deubiquitination. Nature 2003;424:801–5.
32. Brummelkamp TR, Nijman SM, Dirac AM, Bernards R. Loss of the cylindromatosis tumour suppressor inhibits apoptosis by activating NF-kappaB. Nature 2003;424:797–801.
33. Hacker H, Tseng PH, Karin M. Expanding TRAF function: TRAF3 as a tri-faced immune regulator. Nat Rev Immunol 2011;11:457–68.
34. Mauro C, Pacifico F, Lavorgna A, Mellone S, Iannetti A, Acquaviva R, et al. ABIN-1 binds to NEMO/IKKgamma and co-operates with A20 in inhibiting NF-kappaB. J Biol Chem 2006;281:18482–8.
35. Cohen S, Ciechanover A, Kravtsova-Ivantsiv Y, Lapid D, Lahav-Baratz S. ABIN-1 negatively regulates NF-kappaB by inhibiting processing of the p105 precursor. Biochem Biophys Res Commun 2009;389:205–10.
36. Li S, Wang L, Berman M, Kong YY, Dorf ME. Mapping a dynamic innate immunity protein interaction network regulating type I interferon production. Immunity 2011;35:426–40.
37. Adair SJ, Hogan KT. Treatment of ovarian cancer cell lines with 5-aza-2′-deoxycytidine upregulates the expression of cancer-testis antigens and class I major histocompatibility complex-encoded molecules. Cancer Immunol Immunother 2009;58:589–601.
38. Serrano A, Tanzarella S, Lionello I, Mendez R, Traversari C, Ruiz-Cabello F, et al. Rexpression of HLA class I antigens and restoration of antigen-specific CTL response in melanoma cells following 5-aza-2′-deoxycytidine treatment. Int J Cancer 2001;94:243–51.
39. Krishnadas DK, Shusterman S, Bai F, Diller L, Sullivan JE, Cheerva AC, et al. A phase I trial combining decitabine/dendritic cell vaccine targeting MAGE-A1, MAGE-A3 and NY-ESO-1 for children with relapsed or therapy-refractory neuroblastoma and sarcoma. Cancer Immunol Immunother 2015;64:1251–60.
40. G'Sell RT, Gaffney PM, Powell DW. A20-Binding Inhibitor of NF-kappaB Activation 1 is a Physiologic Inhibitor of NF-kappaB: a molecular switch for inflammation and autoimmunity. Arthritis Rheumatol 2015;67:2292–302.
41. Hu H, Brittain GC, Chang JH, Puebla-Osorio N, Jin J, Zal A, et al. OTUD7B controls non-canonical NF-kappaB activation through deubiquitination of TRAF3. Nature 2013;494:371–4.
42. Bista P, Zeng W, Ryan S, Bailly V, Browning JL, Lukashev ME. TRAF3 controls activation of the canonical and alternative NFkappaB by the lymphotoxin beta receptor. J Biol Chem 2010;285:12971–8.
43. Oberst A, Malatesta M, Aqeilan RI, Rossi M, Salomoni P, Murillas R, et al. The Nedd4-binding partner 1 (N4BP1) protein is an inhibitor of the E3 ligase Itch. Proc Natl Acad Sci U S A 2007;104:11280–5.
44. Fenner BJ, Scannell M, Prehn JH. Identification of polyubiquitin binding proteins involved in NF-kappaB signaling using protein arrays. Biochim Biophys Acta 2009;1794:1010–6.
45. Bian X, McAllister-Lucas LM, Shao F, Schumacher KR, Feng Z, Porter AG, et al. NF-kappa B activation mediates doxorubicin-induced cell death in N-type neuroblastoma cells. J Biol Chem 2001;276:48921–9.
46. Armstrong JL, Veal GJ, Redfern CP, Lovat PE. Role of Noxa in p53-independent fenretinide-induced apoptosis of neuroectodermal tumours. Apoptosis 2007;12:613–22.
47. Feng Z, Porter AG. NF-kappaB/Rel proteins are required for neuronal differentiation of SH-SY5Y neuroblastoma cells. J Biol Chem 1999;274:30341–4.
48. Condello S, Caccamo D, Curro M, Ferlazzo N, Parisi G, Ientile R. Transglutaminase 2 and NF-kappaB interplay during NGF-induced differentiation of neuroblastoma cells. Brain Res 2008;1207:1–8.
49. de Bittencourt Pasquali MA, de Ramos VM, Albanus RDO, Kunzler A, de Souza LHT, Dalmolin RJS, et al. Gene expression profile of NF-kappaB, Nrf2, glycolytic, and p53 pathways during the SH-SY5Y neuronal differentiation mediated by retinoic acid. Mol Neurobiol 2016;53:423–435.

Downloaded from http://aacrjournals.org/cancerres/article-pdf/78/23/6621/2601371/6621.pdf by guest on 12 October 2024